

Inhomogeneous phases in the 3+1-dimensional Nambu-Jona-Lasinio model and their dependence on the regularization scheme

Laurin Pannullo,^{a,*} Marc Wagner^{a,b} and Marc Winstel^a

^a*Institut für Theoretische Physik, Goethe Universität Frankfurt am Main
Max-von-Laue-Str. 1, 60438 Frankfurt am Main, Germany*

^b*Helmholtz Research Academy Hesse for FAIR,
Campus Riedberg, Max-von-Laue-Straße 12, D-60438 Frankfurt am Main, Germany
E-mail: pannulllo@itp.uni-frankfurt.de, mwagner@itp.uni-frankfurt.de,
winstel@itp.uni-frankfurt.de*

In this work we study the 3 + 1-dimensional Nambu-Jona-Lasinio (NJL) model in the mean field-approximation. We carry out calculations using five different regularization schemes (two continuum and three lattice regularization schemes) with particular focus on inhomogeneous phases and condensates. The regularization schemes lead to drastically different inhomogeneous regions. We provide evidence that inhomogeneous condensates appear for all regularization schemes almost exclusively at values of the chemical potential and with wave numbers, which are of the order of or even larger than the corresponding regulators. This can be interpreted as indication that inhomogeneous phases in the 3 + 1-dimensional NJL model are rather artifacts of the regularization and not a consequence of the NJL Lagrangian and its symmetries.

*The 39th International Symposium on Lattice Field Theory,
8th-13th August, 2022,
Rheinische Friedrich-Wilhelms-Universität Bonn, Bonn, Germany*

*Speaker

1. Introduction

In an inhomogeneous chiral phase both chiral symmetry and translational symmetry are broken by a non-zero spatially oscillating chiral condensate. Such a phase is a common feature in four-fermion and related Yukawa type models at non-zero quark chemical potential, e.g. the 1 + 1-dimensional Gross-Neveu model [1] or the 3 + 1-dimensional Nambu-Jona-Lasinio (NJL) model [2–4]. Interestingly, such a scenario might also be realized in QCD, since an investigation based on the functional renormalization group has found a moat regime in the QCD phase diagram [5], which might be a precursor of an inhomogeneous phase [6]. Similarly, Dyson-Schwinger calculations in QCD found an inhomogeneous phase at low temperature and large chemical potential featuring a chiral density wave within the employed truncation [7].

The majority of existing model calculations with focus on inhomogeneous phases are restricted to the mean-field approximation, i.e. neglecting bosonic quantum fluctuations. Recently, however, lattice Monte-Carlo simulations of 1 + 1-dimensional models were successfully carried out and provided evidence that inhomogeneous regimes also exist in full quantum field theories [8–11]. Extending these simulations to 3 + 1-dimensional models that are closer to QCD, such as the 3 + 1-dimensional NJL model, is straightforward from a technical point of view, but computationally very expensive. As a preparatory step it is, thus, appropriate to carry out corresponding lattice mean-field analyses, to test the lattice setup and to clarify possibly existing conceptual questions. In this work we report on such mean-field analyses of the 3 + 1-dimensional NJL model. Since the model is not renormalizable, our main focus has been to clarify, to what extent inhomogeneous phases depend on the regularization scheme. In this way our investigation is similar to the investigation in Ref. [12], but with focus on lattice regularizations.

2. The 3 + 1-dimensional Nambu-Jona-Lasinio model

The action of the 3 + 1-dimensional NJL model in the chiral limit with a quark chemical potential μ at temperature $T = 1/\beta$ is given by

$$S[\bar{\psi}, \psi] = \int d^3x \int_0^\beta dt \left\{ \bar{\psi} (\not{\partial} + \gamma_0 \mu) \psi + G \left[(\bar{\psi} \psi)^2 + (\bar{\psi} i \gamma_5 \boldsymbol{\tau} \psi)^2 \right] \right\}, \quad (1)$$

where $\bar{\psi}$ and ψ are fermion fields with $N_f \times N_c \times N_\gamma = 2 \times 3 \times 4$ components (representing the number of massless flavors, colors and spin components, respectively), G is the coupling of the four-fermion interaction and $\boldsymbol{\tau}$ is the vector of Pauli matrices acting in isospin space.

Introducing bosonic auxiliary fields σ and $\boldsymbol{\pi}$ via a Hubbard-Stratonovich transformation and integrating over the fermion fields leads to the effective action

$$S_{\text{eff}}[\sigma, \boldsymbol{\pi}] = \int d^3x \int_0^\beta d\tau \frac{\sigma^2 + \boldsymbol{\pi}^2}{4G} - \ln \text{Det } D, \quad Z = \int \mathcal{D}\sigma \mathcal{D}\boldsymbol{\pi} e^{-S_{\text{eff}}[\sigma, \boldsymbol{\pi}]}, \quad (2)$$

where

$$D = \not{\partial} + \gamma_0 \mu + m_0 + \sigma + i \gamma_5 \boldsymbol{\tau} \cdot \boldsymbol{\pi} \quad (3)$$

is the Dirac operator. The effective action is real-valued for all values of the chemical potential μ and all field configurations $(\sigma, \boldsymbol{\pi})$ (see e.g. Ref. [13]). The expectation values of the bosonic

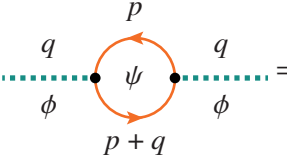
fields satisfy the Ward identities $\langle \bar{\psi}\psi \rangle = -2G\langle \sigma \rangle$ and $\langle \bar{\psi}i\gamma_5\tau_i\psi \rangle = -2G\langle \pi_i \rangle$. One can, thus, study the purely bosonic theory (2) and still obtain insights concerning the chiral condensate and chiral symmetry breaking.

We treat this model in the mean-field approximation. This amounts to considering only a single field configuration $(\sigma, \boldsymbol{\pi})$, which minimizes S_{eff} globally, instead of summing over all field configurations as e.g. in the partition function Z .

The 3 + 1-dimensional NJL model is non-renormalizable, i.e. the regulator cannot be removed via renormalization. The model, thus, has two parameters: the coupling G and the regulator Λ ¹. These parameters are tuned in such a way that the pion decay constant f_π and the constituent quark mass M_0 (in this case the chiral condensate in the vacuum) assume physically motivated values. By choosing $f_\pi = 88$ MeV and varying M_0 in the range 160 . . . 450 MeV we follow a procedure outlined in Refs. [14, 15]. We note that decreasing M_0 leads to increasing Λ .

3. Stability analyses

One can explore the existence of inhomogeneous phases in a comparatively easy and cheap way via stability analyses. The basic idea is to consider arbitrary infinitesimal inhomogeneous perturbations for a given homogeneous field configuration $(\sigma, \boldsymbol{\pi}) = (\bar{\sigma}, \bar{\boldsymbol{\pi}})$ and to determine the curvature of the effective action S_{eff} with respect to these perturbations. If $(\bar{\sigma}, \bar{\boldsymbol{\pi}})$ corresponds to the global homogeneous minimum (i.e. the field configuration from the set of homogeneous field configurations that minimizes S_{eff}), a negative curvature indicates that there is an energetically preferred inhomogeneous condensate. This curvature is given by the bosonic two-point function

$$\begin{aligned} \Gamma_\phi^{(2)}(q) &= \frac{1}{2G} + \text{diagram} = \\ &= \frac{1}{2G} + \int \frac{d^3p}{(2\pi)^3} \frac{1}{\beta} \sum_n \text{tr} \left[S(p+q, \sqrt{\bar{\sigma}^2 + \bar{\boldsymbol{\pi}}^2}) c_\phi S(p, \sqrt{\bar{\sigma}^2 + \bar{\boldsymbol{\pi}}^2}) c_\phi \right], \end{aligned} \quad (4)$$


where ϕ represents one of the four components of $(\sigma, \boldsymbol{\pi})$, $q = (0, \boldsymbol{q})$ is the momentum of the inhomogeneous perturbation, $p = (\omega_n, \boldsymbol{p})$ with ω_n denoting Matsubara frequencies, $S(p, \bar{\sigma})$ is the fermionic propagator, $c_\sigma = \mathbb{1}$, $c_{\pi_j} = i\gamma_5\tau_j$ and tr denotes the trace in isospin, color and spin space. We note that $\Gamma_\sigma^{(2)}(q) = \Gamma_{\pi_j}^{(2)}(q)$ for $(\bar{\sigma}, \bar{\boldsymbol{\pi}}) = 0$.

In Section 5 we present instability regions in the M_0 - μ plane, which are defined by having at least one direction of negative curvature, i.e. where $\Gamma_\phi^{(2)}(q) < 0$ for at least one ϕ and $q \neq 0$. Such instability regions either correspond to or are part of inhomogeneous phases. For a more detailed discussion of stability analyses we refer to Refs. [16–18].

¹In this work we compare several regularization schemes, where each regularization scheme defines the regulator in a different way. For simplicity we denote all regulators by Λ . For example, Λ can represent a momentum cutoff or be proportional to the inverse lattice spacing.

regularization	$S(p, \bar{\sigma})$	momentum integration
Pauli-Villars	$\frac{-i\not{p} + \bar{\sigma}}{p^2 + \bar{\sigma}^2}$	$\frac{1}{\beta} \sum_{n=-\infty}^{\infty} \int d^3p \left(f(\omega_n, \mathbf{p}, \bar{\sigma}) - \sum_{j=1}^{N_{\text{PV}}} a_j f(\omega_n, \mathbf{p}, m_j) \right)$
Spatial momentum cutoff	$\frac{-i\not{p} + \bar{\sigma}}{p^2 + \bar{\sigma}^2}$	$\frac{1}{\beta} \sum_{n=-\infty}^{\infty} \int_0^{2\pi} d\phi \int_0^\pi d\theta \sin\theta \int_0^\Lambda dp p^2 f(\omega_n, \mathbf{p}, \bar{\sigma})$
SLAC	$\frac{-i\not{p} + \bar{\sigma}}{p^2 + \bar{\sigma}^2}$	$\frac{1}{a^4} \sum_{p \in \Gamma_{\text{SLAC}}} f(\omega_n, \mathbf{p}, \bar{\sigma})$
Hybrid with $\tilde{W}_\Theta(p)$	$\frac{-i(\gamma_0 p_0 + \gamma_j \sin(p_j)) + \bar{\sigma}}{p_0^2 + \sin^2(p_i) + \bar{\sigma}^2}$	$\frac{1}{a^4} \sum_{p \in \Gamma_{\text{Hybrid}}} f(\omega_n, \mathbf{p}, \bar{\sigma})$
Hybrid with $\tilde{W}_c(p)$		

Table 1: Summary of the main equations corresponding to the five regularization schemes used in this work: propagator S and momentum integration of a generic function f of the fermionic Matsubara frequencies ω_n , the fermionic momentum \mathbf{p} and a mass $\bar{\sigma}$.

4. Regularization schemes

We carry out computations with two continuum and three lattice regularization schemes, which require different expressions for the propagator S and the integration over fermionic momenta $\int \frac{d^3p}{(2\pi)^3} \frac{1}{\beta} \sum_n$ appearing e.g. in Eq. (4). This is briefly summarized in Table 1.

4.1 Continuum regularization schemes

Pauli-Villars The Pauli-Villars (PV) regularization scheme removes UV-divergencies in momentum integrals by introducing additional propagators with mass $m_j = \sqrt{\bar{\sigma}^2 + \alpha_j \Lambda^2}$. This is sketched in Table 1, where $N_{\text{PV}} \geq 2$ is the number of PV regularization terms, a_j and α_j are coefficients, which have to be properly tuned, and Λ is the so-called PV mass serving as the regulator [14]. We choose $N_{\text{PV}} = 3$, $\mathbf{a} = (1, -3, 3, -1)$ and $\boldsymbol{\alpha} = (0, 1, 2, 3)$. The PV regularization scheme is very common in existing investigations of inhomogeneous phases in NJL-type models (see e.g. Refs. [3, 19]).

Spatial momentum cutoff A spatial momentum cutoff removes UV-divergencies in momentum integrals by limiting the region of integration for spatial momenta to a three dimensional sphere with radius Λ . The summation over Matsubara frequencies is not truncated. This regularization scheme breaks both Euclidean rotational symmetry and translational invariance, even at $T = 0$ and $\mu = 0$.

4.2 Lattice discretizations

SLAC fermions SLAC fermions are common in lattice field theory and are extensively discussed in the literature (see e.g. Ref. [8] and references therein).

Hybrid discretizations This type of lattice discretization combines two standard approaches, the SLAC discretization in the temporal direction and the naive discretization in the three spatial directions. The latter leads to fermion doubling in the spatial dimensions, which can, however, easily be compensated in the mean field approximation by rescaling the coupling. It is, however, mandatory to modify the interaction between fermions and bosons, to suppress unphysical interactions between

the doublers. This requires an appropriate weight function in momentum space, for which we consider two possibilities,

$$\tilde{W}_\Theta(p) = \prod_{\mu=0}^3 \Theta(\pi/2 - |p_\mu|) \quad \text{and} \quad \tilde{W}_c(p) = \prod_{\mu=0}^3 \frac{1 + \cos(p_\mu)}{2}. \quad (5)$$

For details we refer to Refs. [8, 17].

Momentum integration, finite spacetime volume On a finite periodic lattice with $N_t \times N_s^3$ lattice sites and lattice spacing a momentum integrations are replaced by finite sums (see Table 1). The corresponding discrete momenta are

$$\Gamma_{\text{SLAC}} = \left\{ p = \left(\frac{\pi}{N_\mu a} 2n_\mu \right) \mid n_\mu \in \left\{ \frac{N_\mu - 1}{2}, \frac{N_\mu - 3}{2}, \dots, \frac{1 - N_\mu}{2} \right\} \right\} \quad (6)$$

$$\Gamma_{\text{Hybrid}} = \left\{ p = \left(\frac{\pi}{N_\mu a} (2n_\mu + \delta_{\mu,0}) \right) \mid n_\mu \in \left\{ \frac{N_\mu}{2} - 1, \frac{N_\mu}{2} - 2, \dots, \frac{-N_\mu}{2} \right\} \right\}. \quad (7)$$

For the SLAC discretization the number of temporal lattice sites has to be even and the number of spatial lattice sites has to be odd, which corresponds to antiperiodic and periodic boundary conditions, respectively. The Hybrid discretization requires all N_μ to be even. Momenta on the lattice are restricted by $|p_\mu| \leq \pi/a$. We identify the regulator for the SLAC fermions with this upper bound, i.e. define $\Lambda = \pi/a$. For the Hybrid discretization we define $\Lambda = \pi/(2a)$ in order to reflect the effective doubling of the lattice spacing by the fermion doubling.

Momentum integration, infinite spacetime volume On an infinite lattice

$$\int \frac{d^3 p}{(2\pi)^3} \frac{1}{\beta} \sum_n \rightarrow \int_{-\pi/a}^{+\pi/a} dp_0 \int_{-\pi/a}^{+\pi/a} dp_1 \int_{-\pi/a}^{+\pi/a} dp_2 \int_{-\pi/a}^{+\pi/a} dp_3, \quad (8)$$

i.e. a sum over Matsubara frequencies is replaced by an integral and the integration range is hypercubic. It is straightforward to solve such integrals numerically. Thus, we can perform calculations at $T = 0$ and infinite spatial volume.

5. Results

In this section we present results from computations carried out with different regularization schemes, as discussed in Section 4. Unless explicitly stated otherwise, we consider $T = 0$ and set $f_\pi = 88 \text{ MeV}$.

We obtain homogeneous phase boundaries (separating global homogeneous minima with $(\bar{\sigma}, \bar{\boldsymbol{\pi}}) \neq 0$ at small chemical potential from those with $(\bar{\sigma}, \bar{\boldsymbol{\pi}}) = 0$ at larger chemical potential) and instability regions in the M_0 - μ plane as shown in Fig. 1. The key observations are the following:

- (a) Results obtained with different regularization schemes are in fair agreement for large values of Λ (corresponding to values of M_0 , which are much smaller than the physically motivated range). This is expected, since, in general, results obtained with different regularization

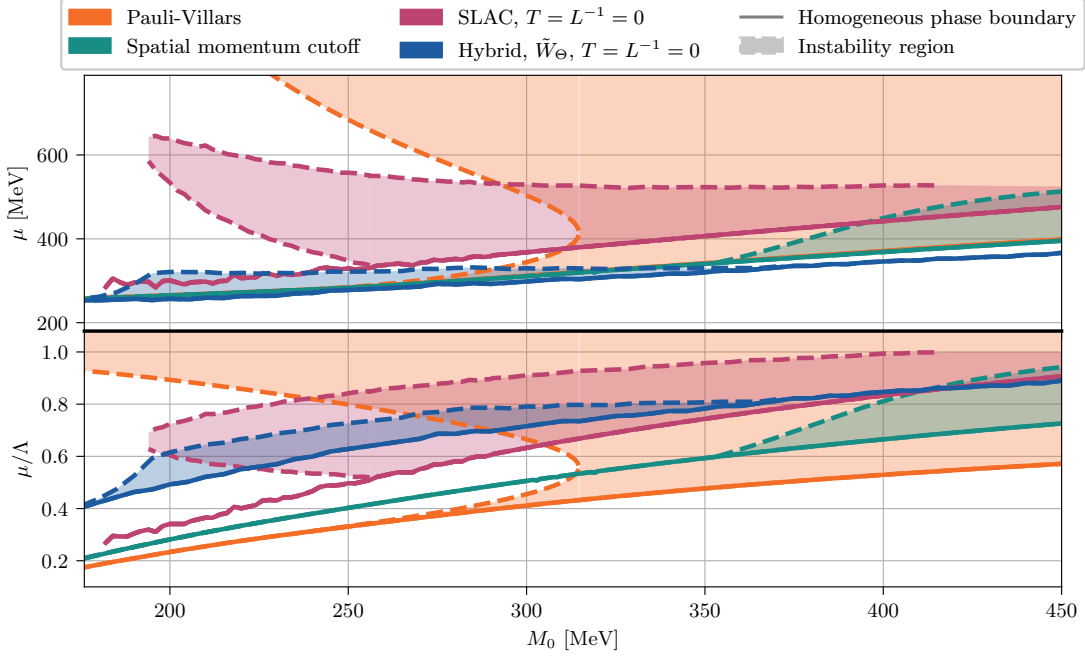


Figure 1: Homogeneous phase boundaries and instability regions in the M_0 - μ plane (upper plot) and in the M_0 - μ/Λ plane (lower plot) obtained with different regularization schemes for $T = 0$ and $f_\pi = 88$ MeV. For the Hybrid discretization with weight function \tilde{W}_c there is only a homogeneous phase boundary, but no instability region. This homogeneous phase boundary is identical to that of the Hybrid discretization with weight function \tilde{W}_Θ and, thus, not shown in a separate color. Integrals (8), appearing for the lattice regularization schemes, were evaluated with statistical methods, resulting in boundaries, which exhibit small statistical fluctuations.

schemes should converge to one another for sufficiently large values of their regulators. However, for such large values of Λ , regions of instability do not exist².

(b) Four of the five regularization schemes lead to instability regions, which are drastically different. In these regions the corresponding chemical potentials are, however, of the same order or even larger than Λ (see in particular the lower plot in Fig. 1).

(c) For the Hybrid discretization with weight function \tilde{W}_c a region of instability does not exist.

From (b) and (c) we conclude that instability regions are closely related to the regulator and strongly dependent on the regularization scheme.

To investigate this further, we define

$$Q = \begin{cases} \operatorname{argmin}_{\phi, q>0} \Gamma_\phi^{(2)}(q) & \text{if } \min_{\phi, q>0} \Gamma_\phi^{(2)}(q) < 0 \\ 0 & \text{else} \end{cases}, \quad (9)$$

where $\Gamma_\phi^{(2)}$ is the two-point function (4). A value of $Q > 0$ indicates that the condensate is unstable with respect to inhomogeneous perturbations with momenta around Q (the negative curvature of

²An exception is the disconnected instability region at very large values of μ obtained with the PV regularization – the so-called inhomogeneous continent [20].

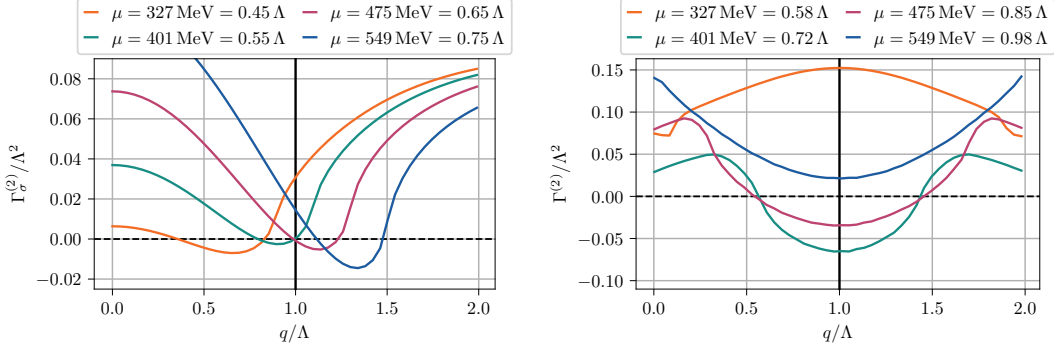


Figure 2: Two-point function $\Gamma_\sigma^{(2)}$ as function of the momentum q for $T = 0$, $f_\pi = 88$ MeV and $M_0 = 325$ MeV obtained with the PV regularization (left) and the SLAC discretization (right).

the effective action is maximized by $q = Q$). Arguments not specific to the NJL model, which are based on quark-hole pairing [20], suggest $Q \approx 2\mu$. This expectation is crudely fulfilled, when using the PV regularization as illustrated by the left plot of Fig. 2, where $\Gamma_\sigma^{(2)}$ is shown as function of q for $M_0 = 325$ MeV and several values of μ . Note, however, that the momenta ranges associated with instabilities, in particular the momenta Q , are of the same order as the regulator Λ . The two-point function is symmetric in q and when using a lattice discretization, $\Gamma_\phi^{(2)}$ is $2\pi/a$ periodic. It is thus sufficient to consider momenta $0 \leq q \leq \pi/a$ with the lattice discretizations³. For the SLAC discretization instabilities are present, with corresponding momenta as well close to Λ (see the right plot of Fig. 2). In particular, $Q = \Lambda$.

Closely related is Fig. 3, where Q is shown in the M_0 - μ plane for the PV regularization and for the two lattice discretizations, where instability regions are found (SLAC and Hybrid with weight function \tilde{W}_Θ). Both lattice discretizations lead almost exclusively to either $Q = 0$, i.e. no instabilities, or to $Q = \Lambda$, i.e. instabilities with preferred momenta close to the regulator. The PV regularization, on the other hand, leads to instability regions, where $Q \approx 2\mu$. However, the preferred momenta are again close to the regulator or even larger, i.e. $Q > \Lambda$.

Item (b) discussed above and the results collected in Fig. 2 and in Fig. 3 complement each other and provide evidence, that both μ and Q , two quantities closely related to the appearance of inhomogeneous phases, are of similar magnitude or larger than the regulator Λ . This raises doubts concerning the physical implication of results on inhomogeneous phases in the NJL model and explains that different regularizations lead to drastically different instability regions (see Fig. 1).

Lattice field theory offers the possibility to go beyond simple stability analyses by minimizing the effective action (2) with respect to σ and $\boldsymbol{\pi}$. Such minimizations can be done numerically without providing specific ansätze for the fields. We present corresponding results for $T = L^{-1} \approx 7.4$ MeV (L denotes the extent of the 3 periodic spatial dimensions), i.e. an $N_t \times N_s^3 = 30 \times 29^3$ lattice, $f_\pi = 88$ MeV, $M_0 = 238$ MeV and $\mu = 442$ MeV in the left plot of Fig. 4. Modulations were restricted to only one of the three spatial directions to limit the computational costs. The energetically preferred field configuration corresponds to $\boldsymbol{\pi} = 0$, but to an oscillating σ with wave length

³The upper bound π/a corresponds to Λ and 2Λ for the SLAC and Hybrid discretization respectively.

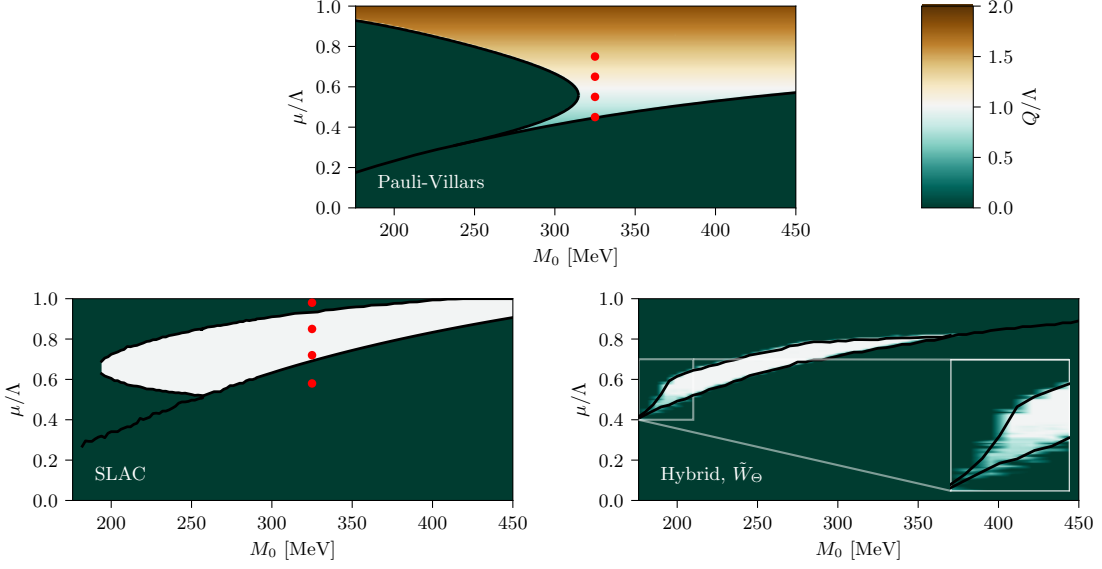


Figure 3: Q in the M_0 - μ plane for three different regularizations for $T = 0$ and $f_\pi = 88$ MeV. Red dots represent the curves from Fig. 2.

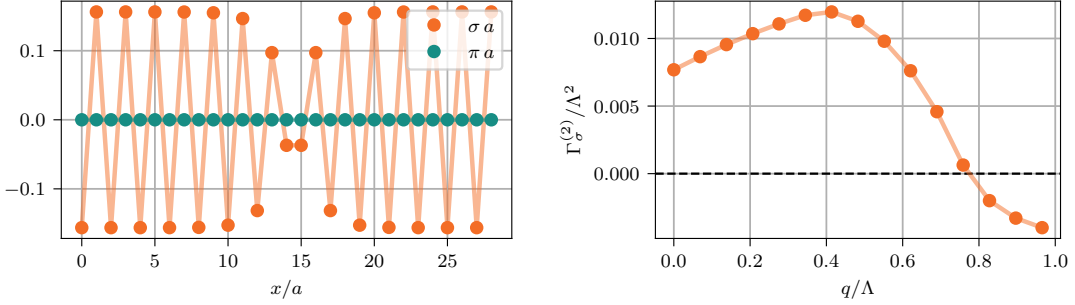


Figure 4: SLAC regularization, $T = L^{-1} \approx 7.4$ MeV, $f_\pi = 88$ MeV, $M_0 = 238$ MeV and $\mu = 442$ MeV. **(left)** Energetically preferred field configuration $(\sigma, \boldsymbol{\pi})$ as function of the spatial coordinate x (arbitrary modulations were allowed in x direction). **(right)** Two-point function $\Gamma_\sigma^{(2)}$ as function of the momentum q .

$2a = 2\pi/\Lambda$, which is the smallest realizable wave length on a lattice. This is another clear sign that the resulting inhomogeneous σ condensate is not physically meaningful, but closely connected to the regulator. For completeness we show the corresponding two-point function $\Gamma_\sigma^{(2)}$ evaluated at the global homogeneous minimum $\bar{\sigma} = \bar{\pi}_i = 0$ in the right plot of Fig. 4. It is qualitatively similar to the two-point functions at $T = 0$ (see Fig. 2). In particular the minimum is again at $Q = \Lambda$.

We note that the results presented in this section are in certain aspects similar to results obtained in the 2 + 1-dimensional Gross-Neveu model [17, 18, 21]. In these references unphysical instability regions and inhomogeneous phases were obtained with the PV regularization and the Hybrid discretization with weight function \tilde{W}_Θ . It was also shown that these instability regions and inhomogeneous phases are only present at finite values of the regulators and disappear after

renormalization.

To summarize, the results presented in this section indicate that existing results on inhomogeneous phases in the 3 + 1-dimensional NJL model should be taken with caution, in particular, when only a single regularization scheme was used. Instability regions seem to be closely related to the regulator, which could be an indication that inhomogeneous phases are rather generated by the regularization and not by the NJL Lagrangian and the symmetries it shares with QCD. Thus, it seems questionable, whether such results have any implication or could provide hints on the existence of inhomogeneous phases in QCD.

Acknowledgments

We acknowledge useful discussions with J. Braun, M. Buballa, Ph. de Forcrand, A. Koenigstein, L. Kurth, J. Lenz, M. Mandl, G. D. Moore, J. Pawłowski, O. Philipsen, F. Rennecke and A. Wipf. This work was supported by the Deutsche Forschungsgemeinschaft (DFG, German Research Foundation) – project number 315477589 – TRR 211. M. Wagner acknowledges support by the Heisenberg Programme of the Deutsche Forschungsgemeinschaft (DFG, German Research Foundation) – project number 399217702. M. Winstel acknowledges support by the GSI Forschungs- und Entwicklungsvereinbarungen (GSI F&E) and by the Giersch Foundation. Calculations on the GOETHE-HLR and on the on the FUCHS-CSC high-performance computers of the Frankfurt University were conducted for this research. We would like to thank HPC-Hessen, funded by the State Ministry of Higher Education, Research and the Arts, for programming advice.

References

- [1] M. Thies and K. Urlichs, *Revised phase diagram of the Gross-Neveu model*, *Physical Review D* **67** (2003) 125015 [[hep-th/0302092](#)].
- [2] E. Nakano and T. Tatsumi, *Chiral symmetry and density wave in quark matter*, *Physical Review D* **71** (2005) 114006 [[hep-ph/0411350](#)].
- [3] D. Nickel, *Inhomogeneous phases in the Nambu-Jona-Lasinio and quark-meson model*, *Physical Review D* **80** (2009) 074025 [[0906.5295](#)].
- [4] M. Sadzikowski and W. Broniowski, *Non-uniform chiral phase in effective chiral quark models*, *Physics Letters B* **488** (2000) 63 [[hep-ph/0003282](#)].
- [5] W.-j. Fu, J.M. Pawłowski and F. Rennecke, *The QCD phase structure at finite temperature and density*, *Physical Review D* **101** (2020) 054032 [[1909.02991](#)].
- [6] R.D. Pisarski and F. Rennecke, *Signatures of Moat Regimes in Heavy-Ion Collisions*, *Physical Review Letters* **127** (2021) 152302 [[2103.06890](#)].
- [7] D. Müller, M. Buballa and J. Wambach, *Dyson-Schwinger study of chiral density waves in QCD*, *Physics Letters B* **727** (2013) 240 [[1308.4303](#)].

- [8] J. Lenz, L. Pannullo, M. Wagner, B. Wellegehausen and A. Wipf, *Inhomogeneous phases in the Gross-Neveu model in $1+1$ dimensions at finite number of flavors*, *Physical Review D* **101** (2020) 094512.
- [9] J.J. Lenz, L. Pannullo, M. Wagner, B. Wellegehausen and A. Wipf, *Baryons in the Gross-Neveu model in $1+1$ dimensions at finite number of flavors*, *Physical Review D* **102** (2020) 114501 [2007.08382].
- [10] J.J. Lenz, M. Mandl and A. Wipf, *Inhomogeneities in the 2 -Flavor Chiral Gross-Neveu Model*, *arXiv:2109.05525 [cond-mat, physics:hep-lat, physics:hep-th]* (2021) [2109.05525].
- [11] C. Nonaka and K. Horie, *Inhomogeneous phases in the chiral Gross-Neveu model on the lattice*, *PoS LATTICE2021* (2022) 150.
- [12] T.L. Partyka and M. Sadzikowski, *Phase diagram of the non-uniform chiral condensate in different regularization schemes at $T=0$* , *Journal of Physics G: Nuclear and Particle Physics* **36** (2009) 025004 [0811.4616].
- [13] S. Hands, B. Lucini and S. Morrison, *Numerical Portrait of a Relativistic Thin Film BCS Superfluid*, *Physical Review D* **65** (2002) 036004 [hep-lat/0109001].
- [14] S.P. Klevansky, *The Nambu-Jona-Lasinio model of quantum chromodynamics*, *Reviews of Modern Physics* **64** (1992) 649.
- [15] S. Hands and D.N. Walters, *Numerical Portrait of a Relativistic BCS Gapped Superfluid*, *Physical Review D* **69** (2004) 076011 [hep-lat/0401018].
- [16] A. Koenigstein, L. Pannullo, S. Rechenberger, M. Winstel and M.J. Steil, *Detecting inhomogeneous chiral condensation from the bosonic two-point function in the $(1+1)$ -dimensional Gross-Neveu model in the mean-field approximation*, *Journal of Physics A: Mathematical and Theoretical* **55** (2022) 375402 [2112.07024].
- [17] M. Buballa, L. Kurth, M. Wagner and M. Winstel, *Regulator dependence of inhomogeneous phases in the $2+1$ -dimensional Gross-Neveu model*, *Physical Review D* **103** (2021) 034503 [2012.09588].
- [18] M. Winstel and L. Pannullo, *Stability of homogeneous chiral phases against inhomogeneous perturbations in $2+1$ dimensions*, Nov., 2022. 10.48550/arXiv.2211.04414.
- [19] A. Heinz, F. Giacosa, M. Wagner and D.H. Rischke, *Inhomogeneous condensation in effective models for QCD using the finite-mode approach*, *Physical Review D* **93** (2016) 014007 [1508.06057].
- [20] M. Buballa and S. Carignano, *Inhomogeneous chiral condensates*, *Progress in Particle and Nuclear Physics* **81** (2015) 39 [1406.1367].
- [21] R. Narayanan, *Phase diagram of the large N Gross-Neveu model in a finite periodic box*, *Phys. Rev. D* **101** (2020) 096001.